Geophys. J. Int. (2006) **164,** 236–245 doi: 10.1111/j.1365-246X.2005.02843.x

Latent heat effects in subsurface heat transport modelling and their impact on palaeotemperature reconstructions

Darius Mottaghy and Volker Rath

Institute for Applied Geophysics, RWTH Aachen University, Aachen, Germany. E-mail: d.mottaghy@geophysik.rwth-aachen.de

Accepted 2005 October 11. Received 2005 October 11; in original form 2004 June 18

SUMMARY

In cold regions the thermal regime is strongly affected by freezing or melting processes, consuming or releasing large amounts of latent heat. This changes enthalpy by orders of magnitude. We present a numerical approach for the implementation of these effects into a 3-D finite-difference heat transport model. The latent heat effect can be handled by substituting an apparent heat capacity for the volumetric heat capacity of unfrozen soil in the heat transfer equation. The model is verified by the analytical solution of the heat transport equation including phase change.

We found significant deviations of temperature profiles when applying the latent heat effect on forward calculations of deep temperature logs. Ground surface temperature histories derived from synthetic data and field data from NE Poland underline the importance of considering freezing processes. In spite of its limitations, the proposed method is appropriate for the study of long-period climatic changes.

Key words: finite-difference methods, geothermics, inversion, palaeoclimate.

1 INTRODUCTION

Frozen soils mainly occur in the polar regions and in the higher reaches of the mountains. The associated thermal regime is called 'permafrost' (Muller 1945). According to the general definition by Lunardini (1981) the term permafrost is used, if the soil shows a temperature at or below 0°C continuously for a significantly long time, but not necessarily for an entire geological period. However, there is no defined time period during which the temperature of the material must remain in the mentioned range. Soils freezing in an exceptional cold winter and persisting over 1 or 2 yr are not classified as permafrost.

The existence of permafrost is a result of the history and the present state of the energy balance at the Earth's surface—measured by the surface temperature—and the deep Earth heat flow. The dominant physical processes in frozen soils are thawing/freezing of water with the release/consumption of latent heat. Furthermore the hydrology is greatly influenced by the frozen soil as the infiltration decreases and long-range run-offs are caused. The quantitative understanding of these mechanism is of paramount importance in order to forecast the results of a climate change, as well as to improve the parametrization of models describing the soil–atmosphere interactions.

In this paper we describe a simple but effective method for modelling of freezing and thawing processes in the subsurface. This enthalpy method has been used by several authors before (e.g. Galushkin 1997; Lunardini 1987). We have implemented this scheme into a general-purpose reactive transport finite-difference code simulating a wide variety of thermal and hydrogeological problems in two and three dimensions. This code, SHEMAT (Simulator for HEat and MAss Transport, Clauser 2003), solves coupled problems involving fluid flow, heat transfer, species transport and chemical water–rock interaction in fluid-saturated porous media. This work extends the application field to thermal systems, where freezing processes become important. The effects of freezing and thawing are particularly interesting when studying ground surface temperature histories (GSTH). Changes in surface temperature with time diffuse into the subsurface, producing characteristic signatures in borehole temperature logs. From these signals the original surface temperature changes can be reconstructed by inverse methods (e.g. Shen & Beck 1991; Mareschal & Beltrami 1992; Beltrami *et al.* 1995; Huang *et al.* 2000). For this purpose we have also used this approach within an inverse code based on 1-D finite-difference forward model. Though the effects on flow phenomena have been included in the SHEMAT modelling code, we will restrict ourselves to the conductive effects in this article, studying synthetic and real data. The effects of freezing/thawing on groundwater flow will be treated in a subsequent article.

2 NUMERICAL MODELLING OF PERMAFROST

A detailed analysis of freezing processes including coupled heat and mass transport in soils is very complex and the theory is not yet fully understood. Because of the non-linearity of the heat transport equation with phase change, and particularly because of the complex coupling between thermal and hydrological processes on one hand

and climatological conditions on the other hand, a simplified model is presented.

2.1 Frozen soil physics

For study of subsurface heat transport, the variation of temperature (T) with time (t) can be described by:

$$\nabla \cdot (\boldsymbol{\lambda} \nabla T - \rho_f c_f T \mathbf{v}) + h = \frac{\partial T}{\partial t}(\phi \rho_f c_f + (1-\phi)\rho_m c_m). \qquad (1)$$

The first term on the left describes the transport of heat by conduction with a thermal conductivity tensor $\boldsymbol{\lambda}$ ($\mathrm{W\,m^{-1}\,K^{-1}}$), whereas the second one specifies advection by motion of pore fluid with a Darcy velocity v ($\mathrm{m\,s^{-1}}$). ρ is density ($\mathrm{kg\,m^{-3}}$), c is heat capacity ($\mathrm{J\,K^{-1}\,kg^{-1}}$), and h is volumetric heat production ($\mathrm{W\,m^{-3}}$). The subscripts f and m account for the two-phase mixture between solid rock (m) and fluid-filled pore space (f). This mixture is characterized by porosity ϕ. When modelling the thermal effects of freezing and thawing, obviously eq. (1) has to include three phases: matrix, fluid and ice. To achieve this, the following volume fractions are defined:

$$\phi_m = 1 - \phi, \quad \phi_f = \phi \cdot \Theta, \quad \phi_i = \phi - \phi_f, \qquad (2)$$

where Θ denotes the fraction of pore space occupied by fluid, and an additional ice phase is introduced marked by index i. The constraint $\phi_m + \phi_i + \phi_f = 1$ implies that pore space is saturated.

As an result of the complicated processes in the porous medium, thawing cannot be considered as a simple discontinuity. Θ is generally assumed to be a continuous function of temperature in a specified interval (Lunardini 1987), for example,

$$\Theta = \begin{cases} \exp\left[-\left(\dfrac{T - T_\mathrm{L}}{w} \right)^2 \right] & \text{if} \quad T < T_\mathrm{L} \\ 1 & \text{if} \quad T > T_\mathrm{L}. \end{cases} \qquad (3)$$

This function is shown in Fig. 1, and is characterized by a thawing temperature T_L (liquidus, usually 0°C) and a parameter w (usually $\geq$1 K). This corresponds to a freezing interval $\Delta T = T_\mathrm{L} - T_\mathrm{S} =$ 2 K, where T_S is the freezing temperature (solidus), at which almost all fluid is frozen (dotted line in Fig. 1). However, this range is a user specified parameter, making it possible to analyse a variety of ground conditions. Fig. 2 shows an example for the variation of the temperature with time. Here, the surface is exposed to a fixed temperature of 3°C, resulting in a cooling of the soil below the initial temperature of 0°C. As the freezing occurs within the temperature range $T_\mathrm{L} - T_\mathrm{S}$ the phase transition is not isothermal.

2.2 Apparent heat capacity

Usually the concept of an apparent or effective heat capacity is invoked in order to account for the latent heat associated with thawing and freezing by adding a term to eq. (1) (Kukkonen & Šafanda 2001). On the right-hand side the contribution by fluid and ice, subscript f and i, respectively, can (more generally) be written as the time derivative of fluid enthalpy H_f. During thawing, this fluid enthalpy per unit volume changes according to

$$\Delta H_f = \int (\phi_f \rho_f c_f + \phi_i \rho_i c_i)\, dT - \int \rho_i L\, d\phi_i, \qquad (4)$$

where ϕ_f and ϕ_i are the relative volumes occupied by free and frozen fluid, respectively. L is the specific latent heat (for water $\approx$333.6 $\mathrm{kJ\,kg^{-1}}$). Obviously, a volumetric apparent specific heat

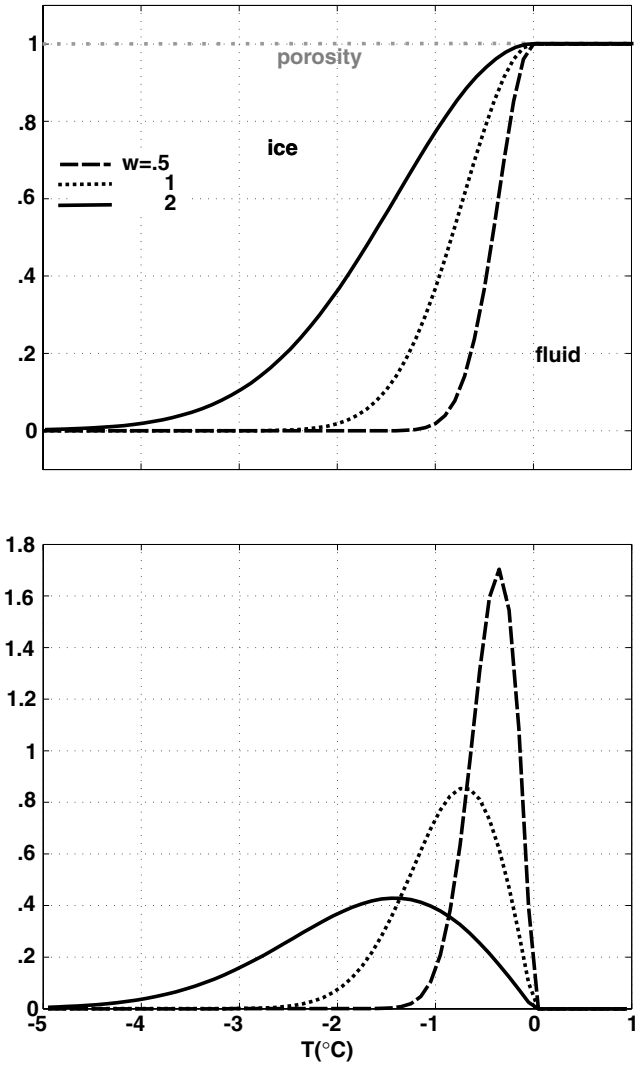

Figure 1. Smooth partition function Θ (top) and its derivative with respect to T (bottom) according to eqs (3) and (8) for several values of the thawing interval w. The area below the curves in the bottom figure are equal, which satisfies the latent heat condition eq. (9).

capacity $(\rho c)_a$ can be defined, which includes additional energy sources or sinks due to latent heat and replaces the fluid contribution of the term in parentheses on the right-hand side of eq. (1):

$$(\rho c)_a = \phi_f \rho_f c_f + \phi_i \rho_i c_i - \frac{\rho_i L d\phi_i}{dT}. \qquad (5)$$

The total derivative in the last term of eq. (5) is usually approximated by a ratio of finite differences, resulting in a constant apparent specific heat:

$$L \frac{\Delta \phi_i}{\Delta T} = L \frac{\phi_{i,L} - \phi_{i,S}}{\Delta T} = \frac{L'}{\Delta T}. \qquad (6)$$

The freezing range is thus described by the temperature interval $\Delta T = T_\mathrm{L} - T_\mathrm{S}$ with fixed temperatures T_S and T_L at which all of the fluid is frozen or unfrozen, respectively (see Section 2.1). This choice leads to an apparent heat capacity of

$$(\rho c)_a = \begin{cases} \phi_f \rho_f c_f & T > T_\mathrm{L} \\ \phi_f \rho_f c_f + \phi_i \rho_i c_i - \dfrac{\rho_i L'}{\Delta T} & T_\mathrm{S} \leq T \leq T_\mathrm{L} \\ \phi_i \rho_i c_i & T \leq T_\mathrm{S}. \end{cases} \qquad (7)$$

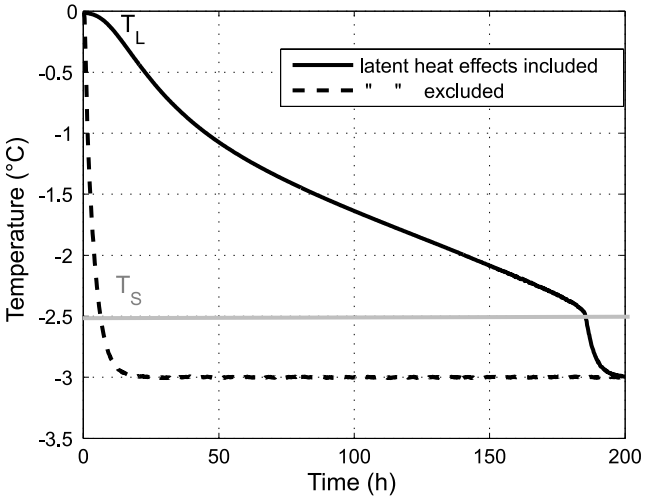

Figure 2. Freezing of soil: an example for a non-isothermal cooling curve due to latent heat, as opposed to instantaneous freezing. The curves show the temperature at 50 cm depth in a homogenous porous medium ($\phi = 0.4$, $\lambda = 2.5$ W m^{-1} K^{-1}). Here, $T_S = 2.5$°C.

Table 1. Temperature, density, specific heat capacity and thermal conductivity of ice at some temperatures (from Miller 1982).

T (°C)	ρ (kg m^{-3})	c_p (kJ kg^{-1} K^{-1})	λ (W m^{-1} K^{-1})
0	916.7	2.11	2.14
−10	918.7	2.03	2.30
−20	920.3	1.96	2.40
−30	921.6	1.88	2.50
−40	922.8	1.80	2.60

In eq. (7), ρ and c are functions of temperature. For the fully unfrozen state the variation with temperature of these are as described in Clauser (2003) and for the fully frozen state properties of ice at different temperatures are taken from Miller (1982) and Lide (2000). Table 1 lists some values for water and ice for comparison. Fig. 3 illustrates, how $(\rho c)_a$ varies with temperature. This approximation of a constant apparent heat capacity is consistent with assuming a ramp function for Θ.

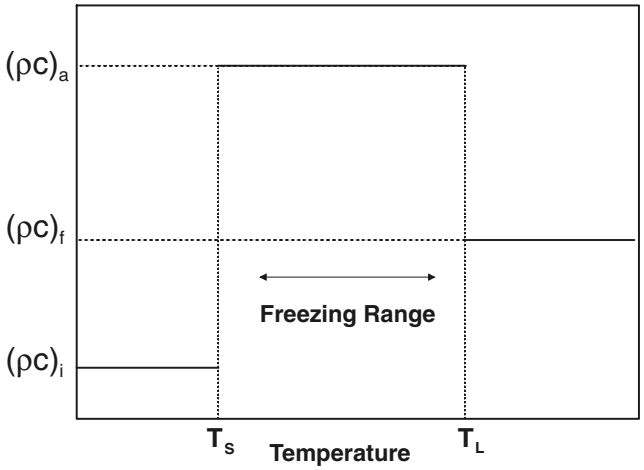

Figure 3. Apparent heat capacity $(\rho c)_a$ as a function of temperature below or above the solidus or liquidus temperature $T_L - T_S$, respectively. Θ is assumed as a ramp function, leading to a piecewise constant $(\rho c)_a$.

As we have chosen a smoother function, we can simply differentiate eq. (3)

$$\frac{d\Theta}{dT} = \begin{cases} -\dfrac{2\,(T - T_L)}{w^2} \exp\left[-\left(\dfrac{T - T_L}{w}\right)^2\right] & \text{if} \quad T \le T_L \\ 0 & \text{if} \quad T > T_L \end{cases} \tag{8}$$

and use this in eq. (5) instead of the approximation in eq. (6). The function Θ and its derivative are shown in Fig. 1.

According to Bonacina & Comini (1973) the actual shape of this curve is not important with regard to the temperature fields calculated, but it must satisfy the latent heat condition,

$$L = \int_{T_S}^{T_L} (\rho c)_a \, dT, \tag{9}$$

which is clearly fulfilled for both choices. The apparent specific heat capacity is a function of temperature, however. Therefore, this approach requires a non-linear solution scheme. For this reason smoother functions for Θ generally improve the convergence of the solution.

2.3 Thermal conductivity

In case of a phase change at a single temperature, thermal conductivity is not continuous with respect to temperature. However, considering the freezing range in rocks, we use eqs (2) and (3) for taking into account the contributions of the fluid and the ice phase. For temperatures below T_S thermal conductivity of ice is assumed to vary linearly with temperature. All other temperature dependencies are accounted for in the original codes. Since the materials are assumed to be randomly distributed, the weighting between them is realized by the square-root mean, which is believed to have a greater physical basis than the geometric mean (Roy *et al.* 1981):

$$\lambda(\phi_{m,f,i}, T) = \left[\phi_m \sqrt{\lambda_m(T)} + \phi_f \sqrt{\lambda_f(T)} + \phi_i \sqrt{\lambda_i(T)}\right]^2. \tag{10}$$

Values for the properties of ice are taken from Miller (1982). Note that other mixing laws may be employed, leading to an corresponding change in eqs (14) and (15).

3 MODEL VERIFICATION

We compare our solutions to a very special case where an analytical solution exists as well as to a more general cases, using other numerical models. All models are purely conductive.

3.1 Analytical solution

The solutions to conductive heat transfer problems with solidification phase change—often referred to as 'Stefan problems' (Stefan 1891)—are inherently non-linear and thus, solution methods are very restricted. A classical solution for a semi-infinite medium with constant temperature undergoing a step change of surface temperature was given by Neumann (ca. 1860) and has been expanded by Carslaw & Jaeger (1959). It is called the Neumann solution and specifies the location $X(t)$ of the phase front (i.e. the isotherm $T = T_S$) as a function of time. At time $t = 0$ the surface $x = 0$ is exposed to a temperature lower than T_S, and it is $T = T_L$ for $x > 0$. Hence it results for the temporal change of the phase front and with it the isotherm $T = T_S$ (see Fig. 4)

$$X(t) = 2\gamma\sqrt{\alpha_i t}, \tag{11}$$

here and in eq. (12) $\alpha_{i,f}$ indicates the thermal diffusivity of ice and water, respectively. The parameter γ must be determined from the

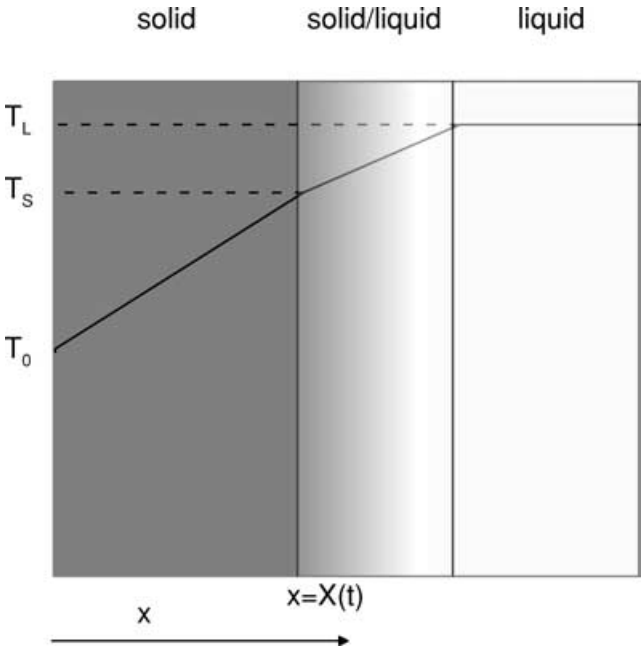

Figure 4. The Neumann problem: location $X(t)$ of the phase front $T = T_S$.

Table 2. The parameter γ for different widths of freezing range.

γ	ΔT (°C)
0.039	4
0.041	3
0.043	2

following equation (Carslaw & Jaeger 1959) that results from the boundary conditions of the associated differential equation (with the thermal conductivities $\lambda_{i,f}$ of both materials):

$$\frac{\exp\left[(\alpha_i - \alpha_f)\gamma^2/\alpha_f\right] erfc\left[\gamma\sqrt{\alpha_i/\alpha_f}\right]}{erf\,\gamma} - \frac{(T_L - T_S)\lambda_f\sqrt{\alpha_i}}{(T_S - T_0)\lambda_i\sqrt{\alpha_f}} = 0. \tag{12}$$

The latent heat effect is considered approximately in eq. (12) by adding the expression of eq. (6) to the thermal diffusivity of the liquid:

$$\alpha_f = \frac{\lambda_f}{\rho_f c_f + \frac{L'}{\Delta T}}. \tag{13}$$

Table 2 lists some computed values of γ for several values of the temperature difference ΔT.

3.1.1 Model properties

A horizontal domain of 20 × 100 nodes and a mesh size of 1 cm is chosen as an approximation for the semi-infinite half-space. The model is purely conductive. Since the analytical solution (eq. 11) is strictly valid only for a homogeneous fluid, the porosity must be chosen as large as possible. Here, in a first approximation, a value of 0.95 is chosen. Later, a more realistic porosity of 0.05 will be used, which requires a modification of the analytical solution. The initial temperature of the half-space is the top of the freezing range ($T_L = 0$°C). At $t = 0$ the surface $x = 0$ exposed to a temperature of $T_0 = -3$°C $< T_S$. The other parameters are summarized in Table 3.

Table 3. Verification model parameters.

Parameter	Value
Grid size; Resolution	20 × 100; 1 cm
Temperature	0°C (−3°C at $x = 0$)
Porosity	0.95 and 0.05
Matrix thermal capacity	2.06 MJ m^{-3} K^{-1}
Matrix thermal conductivity	2.9 W m^{-1} K^{-1}
Time step size; Total simulation time	864 s; 100 days and 1.8 days

3.1.2 Results and discussion

Fig. 5 shows the evolution of the phase front $X(t)$. The crosses show the numerical values, the line the analytical solution. In the beginning the numerical solution overestimates the location of the freezing front, but the error decreases with time, becoming lower than 5 per cent after 10 days. At longer times the difference between analytical and numerical solution is even less. The initially significant deviation is due to the rough discretization of the grid and boundary effects, which decrease as the phase front propagates. The error decreases also for smaller time steps. Additional error sources arise from the fact that a porosity of 1.0 cannot be simulated in SHEMAT and the approximation inherent in the choice of the function Θ shown in Fig. 1. Table 4 lists some values of the analytical and numerical solution, as well as the percentage deviation.

Next, the heterogeneous soil structure is taken into account. The thermal conductivity is weighted by the square-root mean (see Section 2.3) and the thermal capacity by the arithmetic mean. Since the properties in eq. (12) refer only to the fully unfrozen (f) or the fully frozen (i) state, it is sufficient to use the porosity ϕ as in eq. (1). Thus, the thermal diffusivity of the fluid becomes from eq. (12)

$$\alpha_f \to \alpha_{f,m} = \frac{\left(\phi\sqrt{\lambda_f} + (1-\phi)\sqrt{\lambda_m}\right)^2}{\phi_f\rho_f c_f + (1-\phi)\rho_m c_m + \frac{\rho_f L'}{\Delta T}} \tag{14}$$

and the thermal diffusivity of ice becomes

$$\alpha_i \to \alpha_{i,m} = \frac{\left(\phi\sqrt{\lambda_i} + (1-\phi)\sqrt{\lambda_m}\right)^2}{\phi_i\rho_i c_w + (1-\phi)\rho_m c_m}. \tag{15}$$

Fig. 6 shows the evolution of the phase front for a porosity of 0.05 using the modified analytical solution compared to the previous case ($\phi = 0.95$). The front propagates faster, because of the lower water

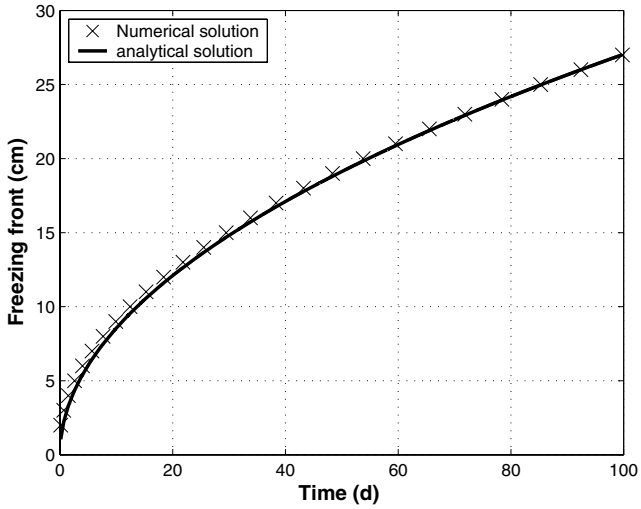

Figure 5. Propagation of the phase front $X(t)$ for the Neumann problem and a porosity $\phi = 0.95$.

Table 4. Location $X(t)$ of the isotherm $T = T_S$ at different times for $\phi = 0.95$ obtained from the analytical and numerical solution.

Time (d)	X_{analyt} (cm)	X_{num} (cm)	Per cent deviation
5	5.4	6	10
20	12.6	13	3.5
50	19.6	20	2.2
80	24.6	25	1.5
99	26.9	27	0.035

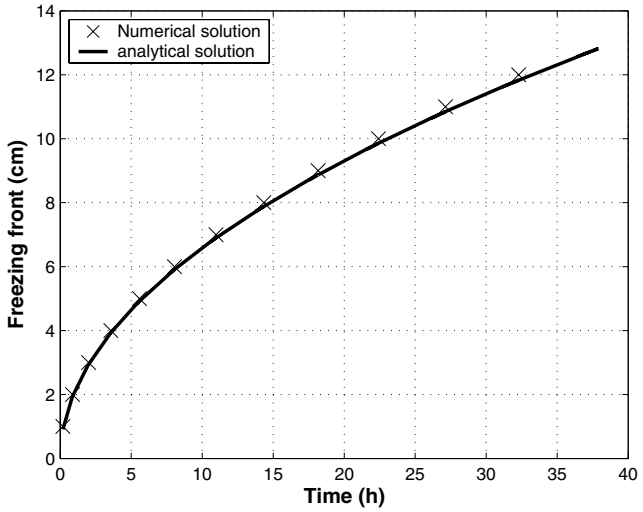

Figure 6. Propagation of the phase front $X(t)$ for the Neumann problem and a porosity $\phi = 0.05$.

content an thus the less latent heat released. Table 5 lists some values of the analytical and numerical solution for comparison.

3.2 Comparison with numerical models

We compare our model to an existing software, GeoStudio™ by GEO-SLOPE International. The module TEMP/W described in GEO-SLOPE™ (2004) is developed for finite element geothermal analysis. It includes Neumann thaw and freeze analysis, for which a similar verification example is given as we have presented in Section 3. Table 6 illustrates the selected parameters for the verification example for TEMP/W. The volumetric water content is idealized and set to 1. The analytical solution assumes a single temperature step for the phase change at 0°C. Since this numerically critical, in TEMP/W a near-perfect stepped function is used, that is, within 0.001°C at temperatures below 0°C the volumetric water content changes from 1 to 0. We keep our model containing a freezing interval from 0°C to −2°C, since we found this method much more numerically stable and define the thaw depth as the −1°C isotherm. Fig. 7 shows the results: the analytical solution given in GEO-SLOPE™ (2004), the

Table 5. Location $X(t)$ of the isotherm $T = T_S$ at different times for $\phi = 0.05$ obtained from the analytical and numerical solution.

Time (h)	X_{analyt} (cm)	X_{num} (cm)	Per cent deviation
8	5.9	6	1.5
18	8.9	9	1.4
22	9.9	10	1.4
27	10.9	11	1.4
32	11.8	12	1.4

Table 6. Parameters of the verification example adapted from TEMP/W.

Parameter	Value
Grid size; Resolution	10 × 500; 1 cm
Ground temperature	−3°C
Surface temperature	5°C
Porosity	0.99
Matrix thermal capacity	2.0 MJ m^{-3} K^{-1}
Matrix thermal conductivity	1.15 W m^{-1} K^{-1}
Total simulation time	1200 d

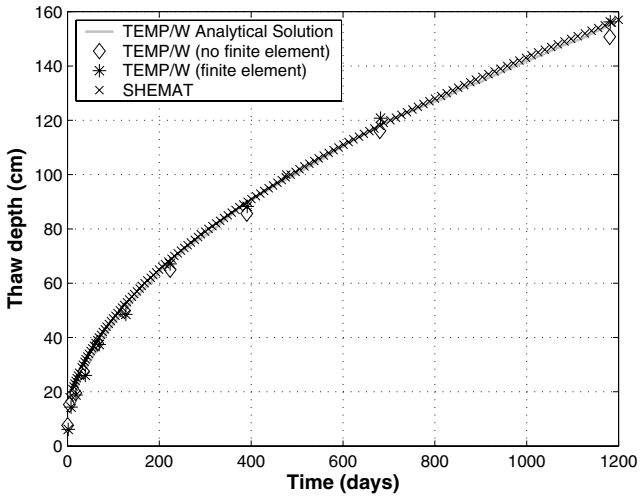

Figure 7. Comparison between SHEMAT and a verification example of the TEMP/W module within GeoSlope™.

numerical solution of TEMP/W, where in one case infinite elements are applied, which is in better agreement with the analytical solution as the latter one assumes a semi-infinite column.

Another comparison with an existing model considers variations in permafrost thickness in response to changes in palaeoclimate. Osterkamp & Gosink (1991) use a step palaeotemperature model for the surface temperature of permafrost for Prudhoe Bay, Alaska, modified from a model by Brigham & Miller (1973). As far as initial and boundary conditions are stated (see Table 7), we implemented them in a SHEMAT model and calculated the permafrost depth, which is defined by Osterkamp & Gosink (1991) as the −1°C isotherm. Since initial and boundary conditions could not be reconstructed completely, there is an absolute shift between both variations of permafrost thickness, which is 200 m. This value was subtracted from the original data of Osterkamp & Gosink (1991), to visualize the good (relative) agreement between the two models; see Fig. 8. According to Osterkamp & Gosink (1991) the observed current thickness of permafrost in Prudhoe Bay is about 600 m, so that our model underestimates the thickness by 14 per cent whereas

Table 7. Parameters of the model adapted from Osterkamp & Gosink (1991).

Parameter	Value
Grid size; Resolution	10 × 900; 1 m
Basal heat flow	0.06 W m^{-2}
Porosity	0.04
Matrix thermal capacity	2.06 MJ m^{-3} K^{-1}
Matrix thermal conductivity	3.39 W m^{-1} K^{-1}
Total simulation time	100 ka

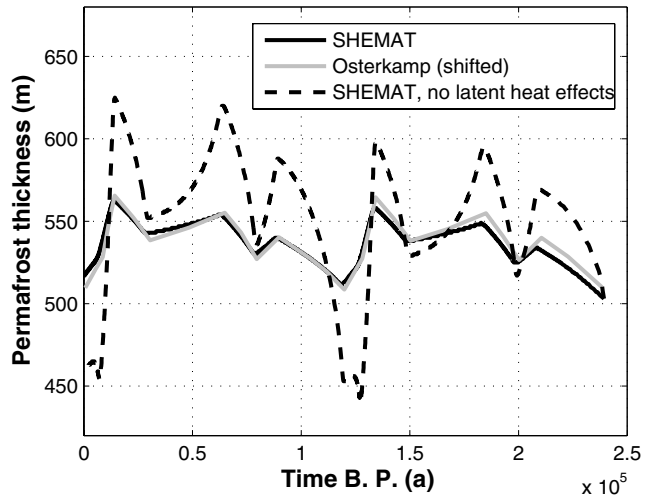

Figure 8. Comparison between the permafrost depth model by Osterkamp & Gosink (1991) and SHEMAT.

the model of Osterkamp & Gosink (1991) yields an 18 per cent higher value. The uncertainty of heat flow is 15 per cent, thus both results are more or less still within the error range.

4 PERMAFROST AND THE RECONSTRUCTION OF PAST SURFACE TEMPERATURES

The inclusion of the latent heat effects is of outstanding importance when analysing the signal of palaeoclimate. This can be done by inverting for GSTH. Here we apply an inversion scheme based on non-linear Tikhonov inversion. Regularization achieved by minimizing the (semi-) norm of a roughening operator applied to the discrete series of temperatures representing GST. The details of this approach are given in a accompanying paper Rath & Mottaghy (in preparation). To deal with permafrost effects, the forward modelling code used in this inversion was replaced with a 1-D implementation of the algorithm described in Section 2.

4.1 Synthetic example

To give a simple example, we used a boxcar time function characterized by a temperature decrease of −9 K (from 1°C) at 65 000 yr before present, returning to 1°C at 15 000 yr before present, marking the fast warming at the end of the last glaciation. The subsurface was assumed to be uniform with respect to petrophysical properties. Fig. 9 shows synthetic temperature logs for different porosities, as well as the maximum deviation induced by the inclusion of permafrost effects.

To demonstrate the effect on palaeoclimate inversions, we chose a high porosity of 30 per cent. As pointed out above, the existence of high porosities are essential for significant permafrost effects. The results are shown in Fig. 10. It is clearly visible from both panels, that under favourable conditions, the effects of permafrost from the last glacial should be visible at depth even now. A recent example for this is given by Šafanda *et al.* (2004), where also independent data are presented supporting the deep occurrence of palaeopermafrost.

Synthetic borehole temperature logs were generated from this simulation, adding normal random noise with a standard deviation of $\sigma = 0.25$ K and a mean of zero. We inverted the resulting data set with, and without permafrost effects included. The difference between including and excluding the latent heat effect in the inversion algorithm is shown in Fig. 11: the sharp increase due to the step function is much better reproduced when inverting with freezing. It has to be remarked, however, that the porosity assumed is rather high. In practice, effects may be smaller or even negligible in crystalline areas. The boxcar forcing function used for the simulation is a hard case for straightforward smoothing inversions, like the one applied here.

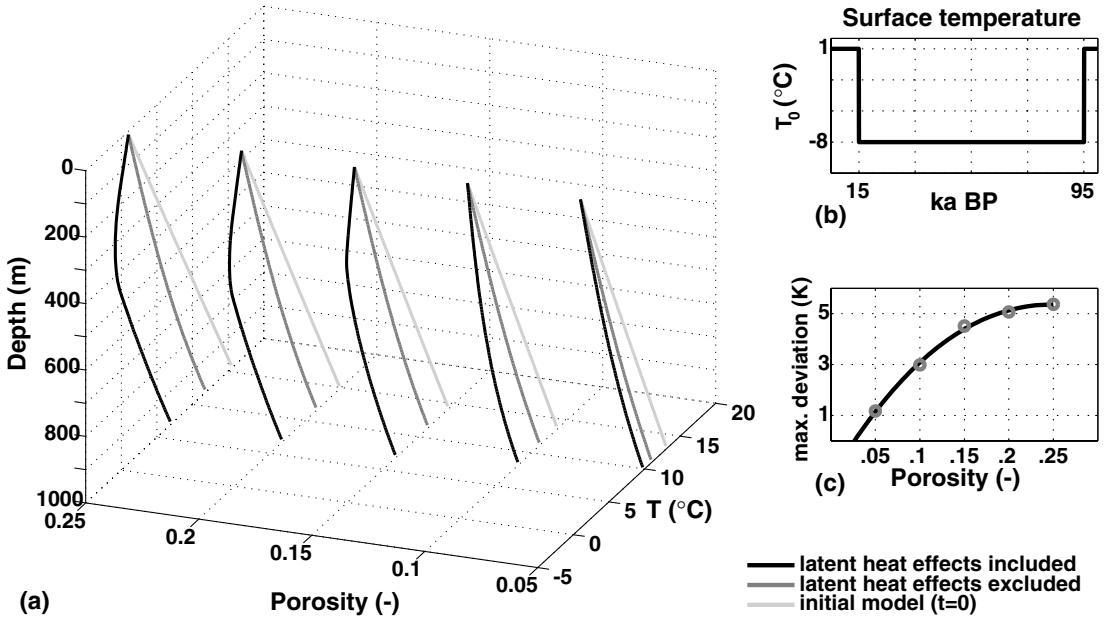

Figure 9. Influence of permafrost formation on ground temperatures for a simple homogeneous model. (a) Temperature profiles for different porosities; (b) Boxcar palaeoclimate forcing function and (c) maximum deviation between models considering and ignoring latent heat effects for different porosities.

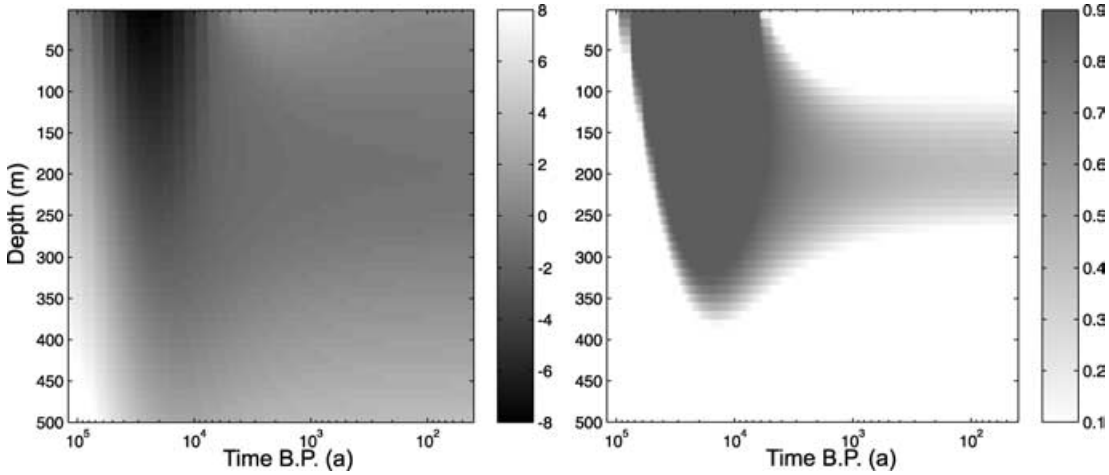

Figure 10. Influence of permafrost formation on ground temperatures for a simple homogeneous model. Left: temperatures in the top 500 m of the model. Right: ice content of the porous medium. A value of 1 implies that all porosity is filled up with ice. It is very clear, that a significant temperature signal or even ice relics can be expected in areas of high porosity.

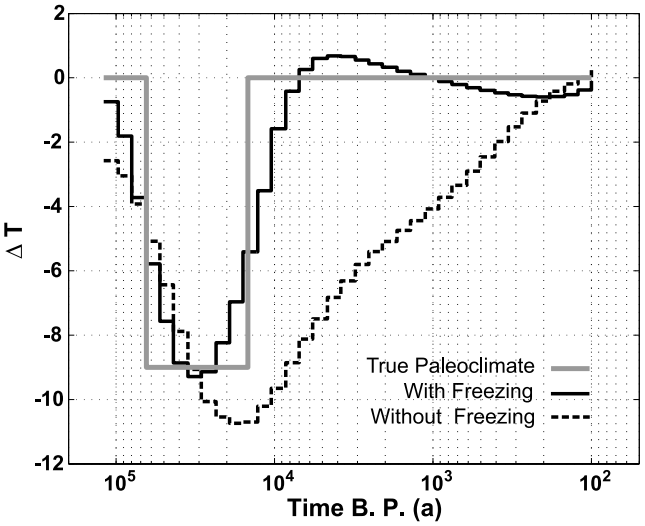

Figure 11. Inversion of a synthetic temperature log, featuring the palaeoclimatic signal of a step function (grey line). Porosity is $\phi = 0.3$.

4.2 Field example

We used this method interpreting temperature data from a borehole, UDRYN IG-8, located in NE Poland. In this borehole not only temperature data were available, but also porosities and thermal conductivities reconstructed from borehole wireline logging. We used a simple layered model compiled by Majorowicz (private communication, 2005). The data for this borehole is shown in Fig. 12. From this figure it becomes obvious that porosity is high enough to expect a significant impact of the thawing/freezing process. For the inversion we had to set the extent of the forward model to a depth of 5000 m, assuming the properties below the depth of the borehole to be mean bedrock properties as found in the borehole below 900 m. For the temperature dependence of the thermal properties we adopted the formulations given by Haenel *et al.* (1988) for thermal conductivity, and Herrmann (1999) for heat capacity. Water properties were calculated as a function temperature and pressure. Ice properties and the freezing function are the same as in the forward code presented above. Boundary conditions were set as follows. At the top we assumed a variable GSTH. The best fit to the borehole data was obtained with a recent mean annual temperature of 7°C, which is slightly above the mean annual air temperature (2 m height) at the location of the borehole (≈6°C). As we took the thermal conductivity to be basically correct, there is not much freedom to vary the basal heat flow, which is 38.4 mW m^{-2} at a depth of 5000 m, accounting for heat production. This corresponds to a surface heat flow of 41.4 mW m^{-2}, which has been determined by Majorowicz (personal communication, 2005). The temperature data were smoothed and interpolated to the grid used for the modelling. We assumed a logarithmic temporal grid, starting with large time steps in the past from 150 ky to small steps up to the present.

From the experience with the inversions we found that the best fit we could obtain increased systematically with depth (see Fig. 13). This suggests that some depth dependent petrophysical parameter variations have not been sufficiently determined. For instance, we used a general relationship for crustal-scale studies for the temperature dependence of thermal conductivity and capacity. The coefficients of these polynomial representations should be adapted to the sedimentary environment at the UDRYN site. Also, heterogeneities at larger depths should be taken into consideration. For this reason, we only used the data above 1500 m of the borehole.

We parametrized the GSTH by a piecewise constant function, with a logarithmic decreasing interval. For the particular inversions shown we limited the degrees of freedom to 64. A logarithmic grid is well adapted for the fact that the temporal resolution of borehole data decreases with age. We ran the inversion with different smoothness constraints which determine the balance between roughness and data fit (Rath & Mottaghy, in preparation). For the results shown below, we chose the regularization parameters to the values corresponding to lowest values producing a stable result. As using a constant prior implies an unrealistic assumption of mean temperatures before the initiation of the simulation, we chose a smooth transition from the recent GST of 7°C to a initial value of −9°C. This particular prior model entering the regularization was inspired by the results of Šafanda *et al.* (2004).

The results from our inversions are given in Fig. 14. Although these inversions may be improved following the suggestions given above, several conclusions can be drawn: given a fixed regularization, the inclusion of latent heat effects improves the data fit significantly. Additionally, the resulting GSTH appears to be more

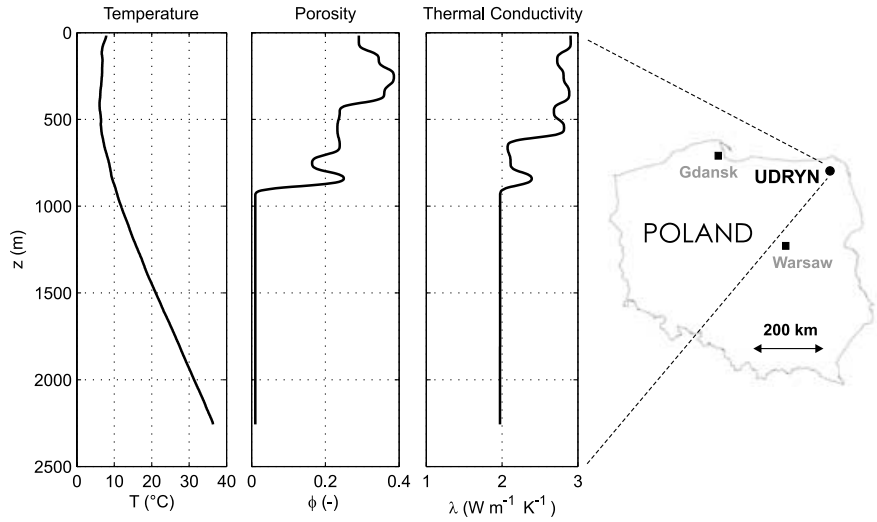

Figure 12. Temperature, porosity, and thermal conductivity from the UDRYN IG-8 borehole. We calculated the matrix thermal conductivity from the available effective property by a geometric mixing law.

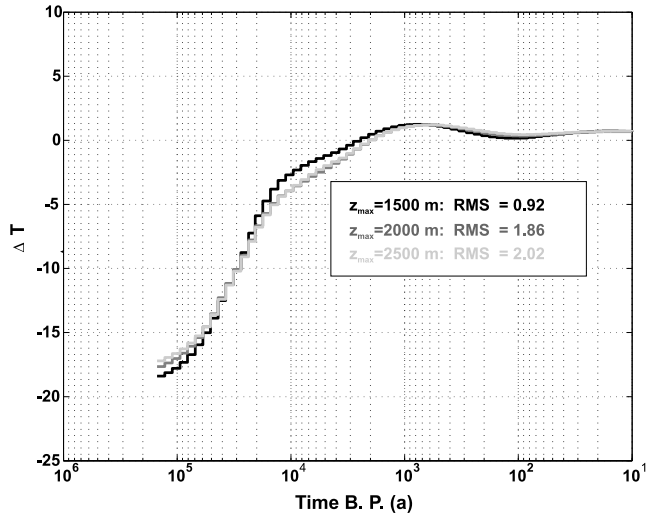

Figure 13. Comparison of inversions of truncated logs from the UDRYN borehole. The best fit could be obtained from the shortest logs. Data fit is measured by RMS $= \sqrt{\frac{1}{N}\frac{(T_{\rm obs}-T_{\rm calc})^2}{\sigma^2}}$.

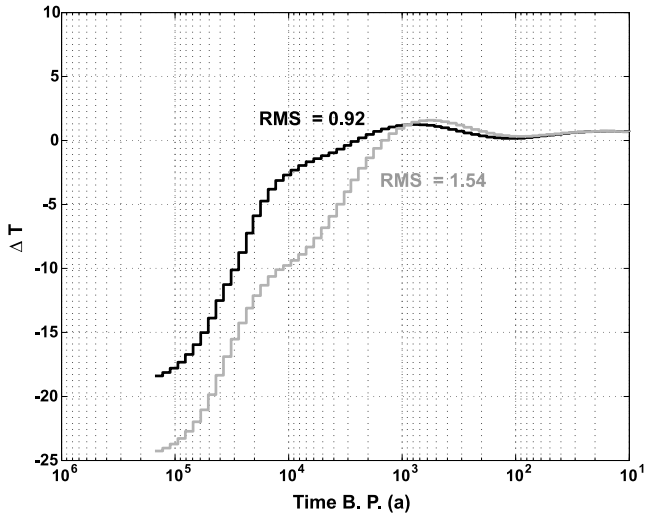

Figure 14. Comparison of the results from the palaeoclimatic inversions for GST from the UDRYN borehole. The black curve represents the results including latent heat effects, while the grey line is the result obtained from standard assumptions. The former shows a better fit to the data, indicated by a much lower RMS. The large effect is mainly due to the very high porosity in the upper 900 m (see Fig. 12). Both curves refer to baseline of 7°C, that is, the zero level corresponds to this value.

consistent with our knowledge on the timing of the end of the Weichselian glaciation some 14–15 ka ago (Hartmann 1994). The lowest temperature resulting from the inversion is about −10°C. From these results we calculated the history of subsurface temperatures and the amount of ice content.

In general, our findings in this study agree well with the results of Šafanda *et al.* (2004), who present forward modelling results including permafrost for the same borehole. The minimum temperature obtained by our inverse model (−10°C) is nearly the same as the one given by these authors. As in their model, permafrost disappeared about 4 ka BP (see Fig. 15). The maximum permafrost depth defined by the −1°C isotherm, however, is larger in our model (≈650 m in contrast to ≈520 m). This is probably due to differences in the assumed temperature dependencies in the thermophysical rock and fluid properties. Additionally, the partition function in eq. (3) is different from the one used by Šafanda *et al.* (2004).

5 CONCLUSION

The model presented includes latent heat effects due to freezing and melting processes in a heat transport model for porous media. In order to facilitate the complex behaviour of freezing processes, various assumptions had to be made. First simulations of heat transport based on this method reveal a considerable influence on thermal properties of soil. It becomes evident that the influence of permafrost development can play a significant role on the subsurface thermal regime, depending on porosity.

The thermal signal of past climate can be reconstructed from recent deep borehole temperatures for the last few ten thousand years. This implies that many areas no longer showing signs of permafrost have seen low temperatures and possibly permafrost during this

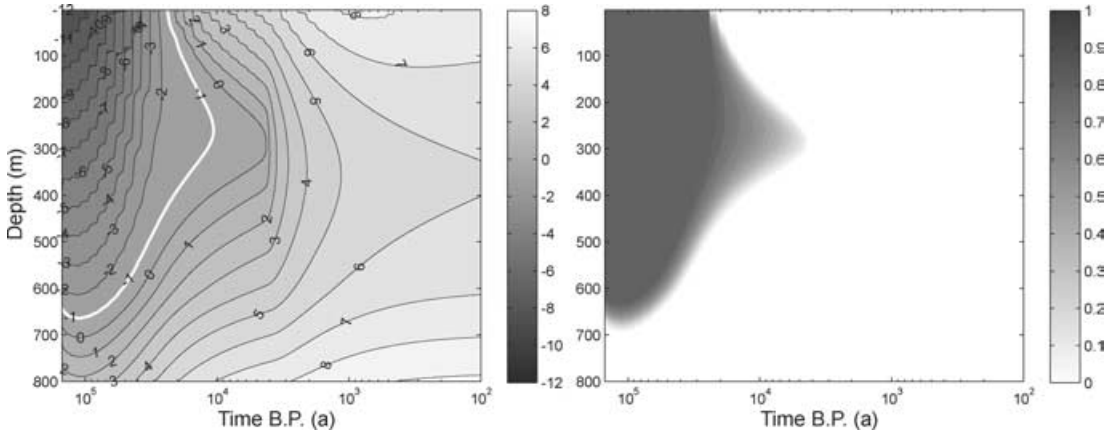

Figure 15. Permafrost formation at the UDRYN site from the inversion model shown in Fig. 14. Left: Temperatures (°C) in the top 800 m of the model. Right: Ice content of the porous medium. A value of 1 implies that all porosity is filled up with ice. Defining permafrost thickness by the −1°C isotherm (white line), it reaches a maximum depth of 650 m shortly after the beginning of the simulation. No ice is present after ≈4 ka BP. The ice content is defined as in Fig. 10. In contrast to this homogenous model, the actual amount of ice and latent heat here depends on the variable porosity.

period. Therefore, the inclusion of the thermal effects of permafrost is essential when aiming at the reconstruction of consistent spatial distributions of past temperatures over large regions. We tested our model on field data, confirming that the freezing/thawing effects yields significantly different results for the inversion results. This implies that wherever high porosities exist, latent heat effects must be considered.

Regional and local fluid flow plays an important role in permafrost regimes. Therefore, in order to be able to investigate these situations, it is also necessary to include flow into our simulations. Only in this way it will be possible to study effects of the coupled influences of forcing climate and fluid flow, which has been shown to be important for a consistent reconstruction of palaeotemperatures (e.g. Kohl 1998).

ACKNOWLEDGMENTS

We thank Jacek Majorowicz for providing the data and information from the UDRYN borehole. We are grateful for valuable comments from the editor Harro Schmeling and the reviewers Hugo Beltrami and Jan Šafanda. DM is working under grant Cl 121/4(1-3) from German Research Foundation (DFG, Bonn) to Christoph Clauser. VR was funded by Bundesamt für Strahlenschutz (BfS, Salzgitter) under contract 9X0009-8390 to RWTH Aachen University.

REFERENCES

Beltrami, H., Chapman, D.S., Archambault, S. & Bergeron, Y., 1995. Reconstruction of high resolution ground temperature histories combining dendrochronological and geothermal data, *Earth planet. Sci. Lett.,* **136,** 437–445.

Bonacina, C. & Comini, G., 1973. On the solution of the nonlinear heat conduction equations by numerical methods, *Int. J. Heat Mass Transfer,* **16,** 581–589.

Brigham, J. & Miller, G., 1973. Paleotemperature estimates of the Alaskan Arctic coastal plain during the last 250,000 years, *Int. J. Heat Mass Transfer,* **16,** 581–589.

Carslaw, H.S. & Jaeger, J.C., 1959. *Conduction of Heat in Solids*, 2nd edn, Clarendon Press, Oxford.

Clauser, C., ed., 2003. *Numerical Simulation of Reactive Flow in Hot Aquifers. SHEMAT and PROCESSING SHEMAT*, Springer, New York.

Galushkin, Y., 1997. Numerical simulation of permafrost evolution as a part of sedimentary basin modeling: permafrost in the Pliocene–Holocene climate history of the Urengoy field in the West Siberian basin, *Canadian Journal of Earth Sciences,* **34,** 935–948.

GEO-SLOPE^{TM}, 2004. *TEMP/W 2004 for Finite Element Geothermal Analysis, Version 5*, `www.geo-slope.com`.

Haenel, R., Rybach, L. & Stegena, L., 1988. *Handbook of Terrestrial Heat-Flow Density Determination*, Kluwer, Dordrecht, Holland.

Hartmann, D.L., 1994. *Global Physical Climatology*, Academic Press, San Diego, California.

Herrmann, H., 1999. Numerische Simulation reaktiver Strömungen im porösen Untergrund am Beispiel der Lösung und Ausfällung, *PhD thesis*, Mathem.–Naturw. Fakultät, Rheinische Friedrich–Wilhelms-Universität Bonn.

Huang, S., Pollack, H.N. & Shen, P.-Y., 2000. Temperature trends over the past five centuries reconstructed from borehole temperatures, *Nature,* **403,** 756–758.

Kohl, T., 1998. Palaeoclimatic temperature signals—can they be washed out?, *Tectonophys.,* **291,** 225–234.

Kukkonen, I.T. & Šafanda, J., 2001. Numerical modelling of permafrost in bedrock in northern Fennoscandia during the Holocene, *Global and Planetary Change,* **29,** 279–273.

Lide, D., ed., 2000. *Handbook of Chemistry and Physics*, 81st edn, CRC Press, Boca Raton.

Lunardini, V.J., 1981. *Heat Transfer in Cold Climates*, Litton Educational Publishing, New York.

Lunardini, V.J., 1987. Freezing of soil with an unfrozen water content and variable thermal properties, *CRREL report 88-2, Nat. Tech. Info. Serv.,* **88-2,** 23.

Mareschal, J.-C. & Beltrami, H., 1992. Evidence for recent warming from perturbed geothermal gradients: examples from eastern canada, *Climate Dynamics,* **6,** 135–143.

Miller, H., 1982. Physical properties of ice, in *Landolt-Börnstein: Numerical Data and Functional Relationships in Science and Technology*, vol. V(B), pp. 482–507, ed. Angenheister G., Springer, Berlin.

Muller, S.W., 1945. Permafrost or permanently frozen ground and related engineering problems, *Special Report, Strategic Engineering Study,* **62,** 136 pp., US Engineering Office.

Neumann, F., ca. 1860. Die Partiellen Differentialgleichungen, *Physik (5th ed., 1912),* **2,** 121.

Osterkamp, T.E. & Gosink, J.P., 1991. Variations in permafrost thickness in response to changes in paleoclimate, *J. geophys. Res.,* **96,** 4423–4434.

Roy, R.F., Beck, A.E. & Touloukian, Y.S., 1981. Thermophysical properties of rocks, in *Physical Properties of Rocks and Minerals*, pp. 409–502, eds Touloukian, Y.S., Judd, W.R. & Roy, R.F., McGraw–Hill, New York.

Shen, P.Y. & Beck, A.E., 1991. Least squares inversion of borehole temperature measurements in functional space, *J. geophys. Res.,* **96,** 19 965–19 979.

Stefan, J., 1891. Über die Theorie des Eisbildens, insbesondere über die Eisbildung im Polarmeere, *Ann. Phys. u. Chem. Neue Folge 42,* **2,** 269–286.

Šafanda, J., Szewzyk, J. & Majorowicz, J.A., 2004. Geothermal evidence of very low glacial temperatures on a rim of the Fennoscandian ice sheet, *Geophys. Res. Lett.,* **31,** L07 211, doi:10.1029/2004GL019 47.